Large Scale Hydrogen Production Using Nuclear Power

David Barbara, Andrew Carmean, Dustin Kraemer and Shripad T. Revankar

School of Nuclear Engineering
Purdue University
West Lafayette, IN 47907

Abstract

Hydrogen production using the Sulfur-Iodine (SI) process coupled to a high temperature gas cooled nuclear reactor was simulated with physical models for the processes. The models included energy balance for the SI process, thermal models for the heat exchanger design, and Brayton cogeneration unit. Process parameters such as mass flow rates of reactor coolant, reactant gases, heat exchanger pipe size, and number of heat exchanger pipes were examined. The computational model predicted that the 265 MW thermal pebble bed modular reactor could produce 17.38 million kg of hydrogen per year. Because excess heat still had to be removed from the helium gas to meet reactor thermalhydraulic specifications, a Brayton cycle was considered as a method of both further cooling the helium gas and producing electricity with overall plant efficiency to 36.3%.

Introduction

The current power generation plants and automotive exhaust have contributed to the environmental pollution and public health problems. These issues together with global and national energy security concerns have generated new ideas for energy production in the last several years including diversification. One of the most promising solutions is hydrogen-based fuel cells. Hydrogen as a carrier of energy is superior to other forms of energy carriers for power generation, transportation and storage. Key challenges for the hydrogen-fuel cell based energy system are the sourcing of hydrogen and development of efficient, affordable and safe production processes.

There is a large demand for the hydrogen and it is increasing at nearly 4-10 percent a year. In the future hydrogen can reduce oil use for transportation and dramatically reduce our reliance on oil. Currently a very small amount of hydrogen is used as a fuel; most of it is used for commercial chemical use. Approximately two-thirds of the hydrogen produced is used for commercial fixation of nitrogen from the air to produce ammonia for fertilizer. Other uses of the hydrogen produced are petroleum refining, hydrogenation of fats and oils, methanol production, in hydrodealkylation, hydrocracking, and hydrodesulphurization, welding, metallic ore reduction, hydrochloric acid production, and the study of liquid hydrogen [1]. In relation to the 9 million tons of hydrogen the US is currently producing per year, approximately 120 million tons of hydrogen per year would be required to replace all of the gasoline use for transportation [2].

Currently known hydrogen production process can be classified into three main methods. The first method is direct electrolysis [3, 4]. The disadvantage of this reaction lies in overall low efficiency. The second class of reactions involves extraction of hydrogen from hydrocarbon such as natural gas, gasoline, diesel and methanol using processes such as steam reforming [5]. These hydrogen sources produce emissions of pollutants and greenhouse gases and thus suffer from some of the same disadvantages attributed to the established power generation methods. The third hydrogen production method can be termed as "intermediate compounds." Processes that did not involve cracking hydrocarbons or direct electrolysis of water fall into this category. In particular, three processes are well known, iron redox reaction [6], sodium borohydride process [7] and SI process [9, 10]. Currently there is much interest in the SI cycle, which was originally proposed by General Atomic (GA) [11, 12] as it has potential for high efficiencies in the hydrogen production [13]. Previous studies based on General Atomics (GA) process indicated the process thermal efficiency of hydrogen production is in the range of 45–50% [12, 14]. Currently there is large interest in Japan in this cycle. The Japan Atomic Energy Research Institute is continuing research in SI process [15-19].

The major advantage of the SI cycle is that it provides a method of producing hydrogen that is environmentally friendly. The major disadvantages of the SI cycle are the high temperature required for the decomposition of hydrogen iodide and the corrosiveness of the reactants. However, high temperature nuclear reactor designs will easily allow a temperature of greater than 800^{o}C. Though SI cycle has been well studied the process has not yet been demonstrated by a commercial, and there seems to remain spaces for further improvement to reduce the complex process scheme. In this regard, the predictive simulations are very useful.

The purpose of this paper was to examine SI cycle coupled to high temperature gas cooled nuclear reactor. A heat-transfer model was developed to analyze the SI process and the coupling of the process to nuclear power reactor. The simulation incorporates the neutronics and thermodynamic analyses of the reactor, analyzes the SI process for given power and provides the overall plant efficiency and hydrogen production rate. The use of nuclear heat from a high temperature gas-cooled reactor as thermal energy for a thermochemical cycle for hydrogen production process has been already considered in the US and Japan [20-22].

2. Nuclear Coupled SI Cycle

The schematic of the hydrogen production facility using SI cycle and nuclear reactor heat is shown in Fig. 1. Amongst the high temperature nuclear reactors, two reactors make good candidates, molten salt or liquid metal cooled high temperature reactor [23] and gas cooled high temperature reactor [24]. The advantage of the latter reactor is the use of a single phase coolant with high temperature capabilities. The system constraints on water cooled reactors limit the coolant (water) to 350^{o}C. Liquid metal reactors are limited in their temperature due to the corrosive properties of the liquid metal at high temperatures leaving the coolant limited to 600^{o}C. Gas cooled reactors are not limited by the coolant capabilities. The gas cooled reactors can reach temperatures over 1000^{o}C, which bring limitations in the form of material issues. The liquid metal reactors produce a high enough coolant temperature to directly drive the SI process; however, losses in a heat exchanger may limit their potential use in providing the energy for this chemical process. To better allow for heat losses in the system before the fluid reaches the SI process, a gas cooled reactor was selected. The high temperature gas cooled reactor considered

is the Eskom design pebble bed modular reactor (PBMR) [25, 26]. The PBMR is capable of temperatures up to 1000°C, which exceeds the 850°C temperature needed to drive the chemical reactions for producing hydrogen. The reactor was separated from the hydrogen production. This allows the reactor to be part of a separate plant linked only by a heat exchanger coupled to the main coolant line. This coupling design allows other reactors to be used instead of the PBMR.

The SI reactions considered consist of three chemical processes, which sum to the dissociation of water.

$I_2(l)+SO_2(g)+2H_20(l) \rightarrow 2HI(aq)+H_2SO_4(aq)$ (120°C) (Process I)

$H_2SO_4(aq) \rightarrow H_2O+SO_2(g)+½O_2(g)$ (850°C) (Process II)

$2HI(g) \rightarrow H_2(g)+I_2(g)$ (450°C)) (Process III)

$H_2O \rightarrow H_2 + ½O_2$ (net reaction)

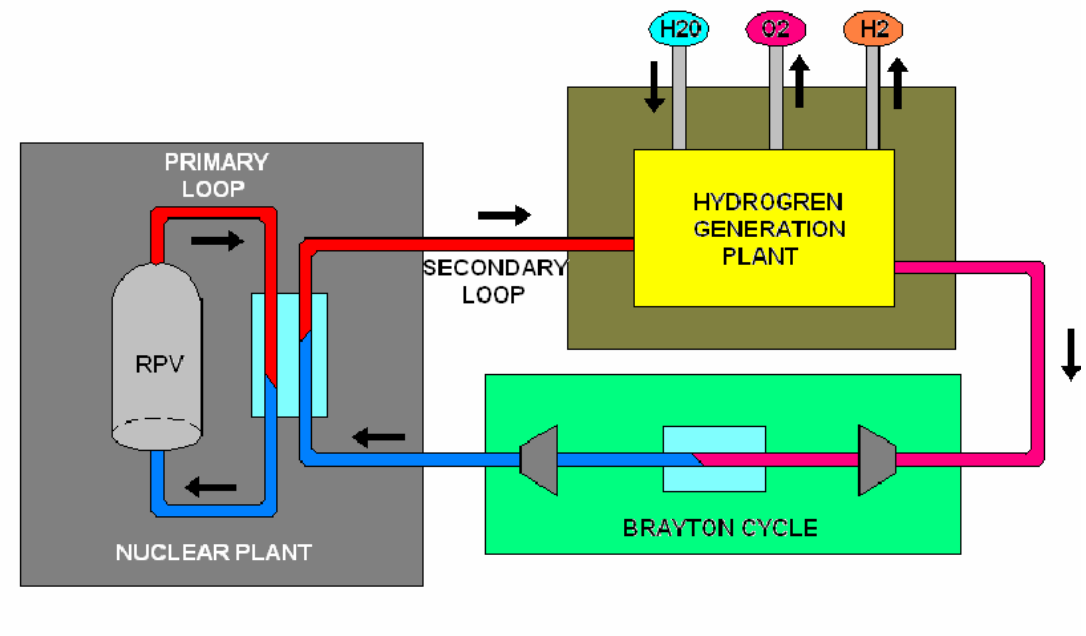

Fig. 1 – Overall plant schematic of hydrogen production facility

The reactions are temperature dependent. With a suitable catalyst, the high-temperature reaction dissociation of sulfuric acid reaches 10% conversion at 510°C, and 83% conversion at 850°C. Energy, as heat, is input to a thermochemical cycle via two main endothermic high-temperature chemical reactions. The heat is rejected via one exothermic low temperature reaction. Most of the input heat goes into the dissociation of sulfuric acid. Sulfuric acid and hydrogen iodide are formed in the endothermic reaction of H_2O, SO_2 and I_2, and the hydrogen is generated in the mildly endothermic decomposition of hydrogen iodide. All the products in this cycle, other than water, are regenerated. Since the reaction products H_2O, SO_2 and I_2 need to be cooled to lower temperature a Brayton cycle is used as co-generation system to enhance the efficiency.

3. Reactor Core Thermal Analysis

The PBMR is 265 MW thermal power reactor with radius of 2.00 meters and height of 5.18 meters consists of UO_2 fuel and a graphite reflector [27]. The active core is a cylinder with radius of 1.00 meters and height of 3.18 meters is surrounded by a ring of absorber material

13cm thick located 6cm away from the core with reflector in-between the two regions. The fuel is a UO_2 of around 9% enrichment. Around 11,000 microspheres with a silicon carbide coating called TRISO fuel particle, make up the 60 millimeter diameter pebbles. The reactor has approximately 380,000 pebbles in its reactor core. The analysis of the core was made using PARCS (Purdue Advanced Reactor Core Simulator) reactor neutronics analysis code [28]. The neutronics model assumed a simplified 2-D approach to the cylindrical calculations. The OTTO (Once Through Then Out) assumption was made for the pebbles in the model. The radial and axial power profiles were obtained with the neutronic calculations as shown in Fig. 2, [27,29]. Using the calculated power profile thermal analysis of the core was carried out. Helium gas was used as coolant for the reactor [27].

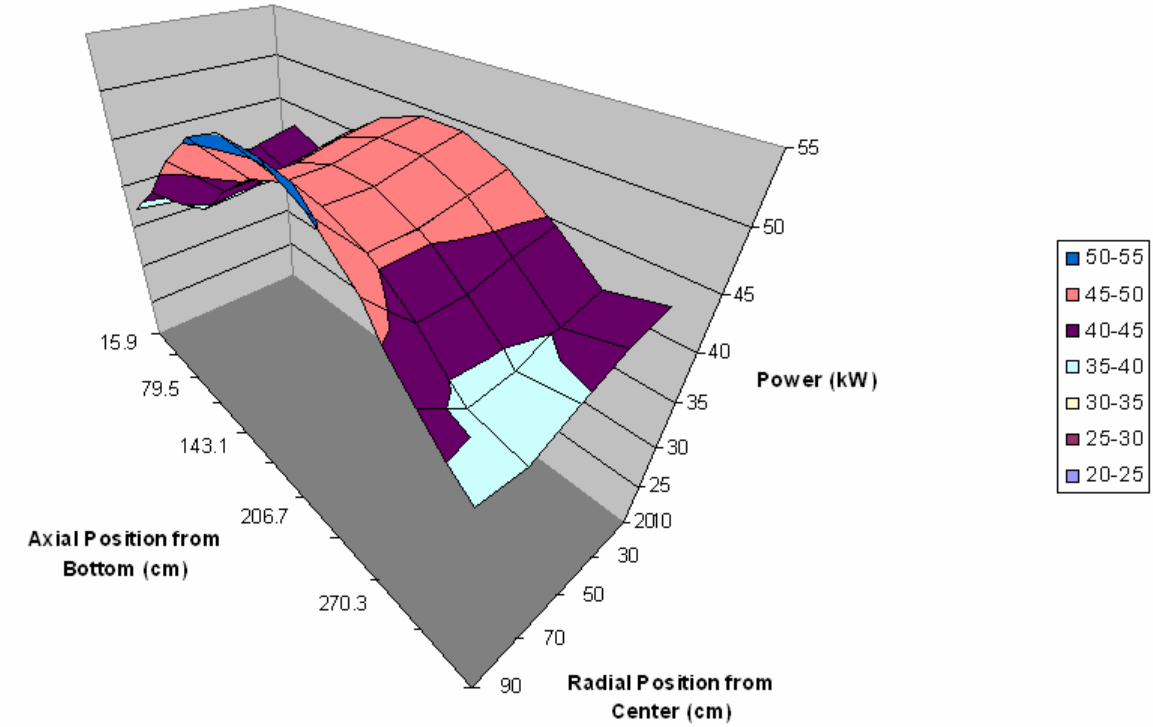

Fig. 2.– Power (in kW) as a function of radial and axial positions.

To calculate the thermal resistance between the center temperature of the pebble and the surface temperature of the pebble, the resistance, R, was modeled as an electric circuit in parallel, where $R=(hA)^{-1}$. Fig. 3, shows the hydraulic model for the pebble bed reactor core. The coolant channel on the right of Fig. 3 is for a light water reactor, while the channel on the left is for the pebble bed reactor.

The porosity, which is the ability to let coolant travel through the channel was considered at conservative value of 40%. The standard correlations were used to analyze the thermalhydraulics of a pebble bed reactor [30]. These correlations are as follows:

$$\Delta P = \Psi\left(\frac{\rho L V^2}{2D_h}\right) \tag{1}$$

where ΔP defines the pressure drop across the pebble, V is the average gas velocity, L is the height of the pebble bed core, ρ is the gas density and ψ is the pressure drop coefficient, which is dependent on the Reynolds number, defined as

$$\Psi = 320\,\mathrm{Re}^{-1} + 6\,\mathrm{Re}^{-0.1}. \quad (2)$$

The Reynolds number is defined as

$$\mathrm{Re} = \left(\frac{1}{1-\varepsilon}\right)\frac{\rho V d_p}{\mu} \quad (3)$$

where d_p is the pebble diameter, ε is the porosity which is conservatively set at 0.4, and μ is the dynamic viscosity. The hydraulic diameter D_h is related to the fuel pebble diameter, d_p given as:

$$D_h = d_p\left(\frac{\varepsilon}{1-\varepsilon}\right) \quad (5)$$

The heat transfer is governed by the Nusselt number correlation :

$$Nu = hd_p / k = \sqrt{0.35\,\mathrm{Pr}^{0.6}\,\varepsilon^{-3.34}\,\mathrm{Re}^{0.87} + 0.00316\,\mathrm{Pr}\,\varepsilon^{-2.05}\,\mathrm{Re}^{1.67}} \quad (6)$$

where h is the heat transfer coefficient and k is the thermal conductivity of the gas.
Relation (6) is valid for $10^2 \le \mathrm{Re} \le 10^5$ and $0.26 \le \varepsilon \le 0.476$.
In the analysis the core of the reactor was split into ten sections axially and five sections radially. By knowing the power in each of the section as well as the area and number of pebbles, the heat flux was found for each section using the equation.

$$q'' = h\left(T_{surface} - T_{bulk}\right) \quad (7)$$

The pebble surface temperature $T_{surface}$ was obtained from the pebble heat transfer model [27] which treated the pebble as a composite material. Using above equations (1)-(7) the heat transfer rate between pebble and the coolant (helium gas) was obtained assuming reactor inlet and outlet temperatures at 500°C and 900°C respectively. While the heat transfer coefficient varies with temperature, the unknown bulk temperature T_{bulk} was found for each section. The gas mass flow rate required was 127.33 kg/s to keep the reactor at steady state.

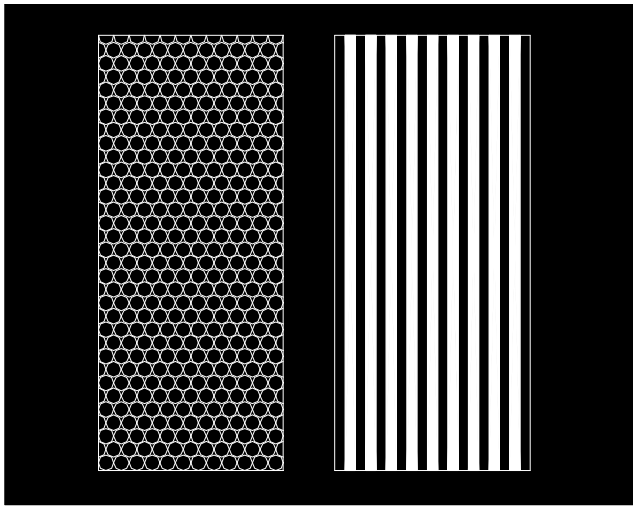

Fig. 3. - PBMR coolant channel schematic [27].

4. SI Process Modeling

The first step in creating a computational model of the SI process in order to analyze the secondary side of the plant was to determine the required energy inputs of the three processes of the entire SI reaction Cycle. The energy input of each reaction involves the reaction enthalpy and the energy required to heat the reactants to the desired temperature. HSC Chemistry 5 [31], was used to analyze the reactions and compute the enthalpy change of each reaction at appropriate temperature ranges of the reaction. After enthalpy of reaction was expressed as a function of temperature, the energy required to heat the reactants to the desired reaction temperature was incorporated to derive the required energy input.

The simplified plant schematic for the hydrogen production process is shown in Fig. 4. For process II, the most endothermic reaction of the SI process, the required energy input was obtained by first determining the enthalpy change of reaction as shown in Fig. 5. The equation of the best fit polynomial for this relation is as follows:

$$\Delta h = \left[-2.1127*10^{-7}T_2^2 - 1.8458*10^{-2}T_2 + 206.43\right]\frac{kJ}{rxn} \tag{8}$$

Here rxn refers to specific reaction.

The heat required to heat the reactant to the temperature of process II, T_2, from the temperature of process I, T_1, was determined by first evaluating the specific heat of the reactant as a function of temperature.
The specific heat of sulfuric acid as a function of temperature was represented as:

$$\bar{c}_p = \frac{1}{2}\left[-1.3860*10^{-5}\left(T_2^2 + T_1^2\right) + 5.3741*10^{-2}\left(T_2 + T_1\right) + 93.037\right]\frac{J}{mol*K} \tag{9}$$

The total required energy input must account for heating of H_2SO_4 from T_1 to T_2 as stated before. The required heat is

$$\Delta h = \bar{c}_p \Delta T = \bar{c}_p\left(T_2 - T_1\right) \tag{10}$$

$$\text{or } \Delta h = \frac{\left(T_2 - T_1\right)}{2*1000}\left[-1.3860*10^{-5}\left(T_2^2 + T_1^2\right) + 5.3741*10^{-2}\left(T_2 + T_1\right) + 93.037\right]\frac{kJ}{rxn} \tag{11}$$

By summing the above result with the enthalpy of reaction demands, the total required heat energy input for Process II is obtained:

$$\begin{aligned} Q = &\left\{-2.1127*10^{-7}T_2^2 - 1.8458*10^{-2}T_2 + 206.43\right\} + \\ &\frac{\left(T_2 - T_1\right)}{2*1000}\left[-1.3860*10^{-5}\left(T_2^2 + T_1^2\right) + 5.3741*10^{-2}\left(T_2 + T_1\right) + 93.037\right]\frac{kJ}{rxn} \end{aligned} \tag{12}$$

Similarly, for Process III, the total required energy input is calculated in the same manner (see Fig. 6.):

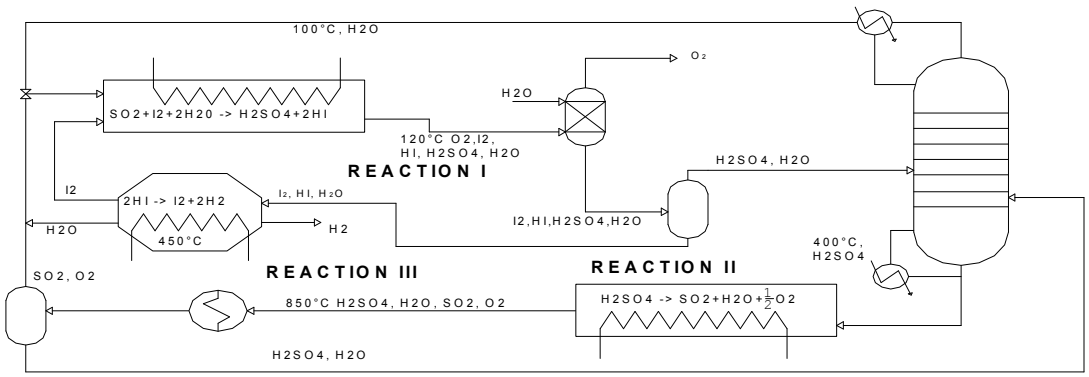

Fig. 4. Simplified plant schematic for the SI Cycle

The enthalpy change of reaction for process III is:

$$\Delta h = \left[-5.0807*10^{-6}T_3^2 + 1.2042*10^{-2}T_3 + 6.4257\right]\frac{kJ}{rxn} \tag{13}$$

The specific heat of HI as a function of temperature was represented as:

$$\bar{c}_p = \frac{1}{2}\left[1.9464*10^{-6}\left(T_3^2 + T_1^2\right) + 4.4086*10^{-3}\left(T_3 + T_1\right) + 27.041\right]\frac{J}{mol*K} \tag{14}$$

The total required energy input must account for the heating of HI from T_1 to T_3:

$$\Delta h = \bar{c}_p \Delta T = \bar{c}_p\left(T_3 - T_1\right) \tag{15}$$

Knowing there are two moles of HI per reaction produces the following equation:

$$\Delta h = \frac{2*\left(T_3 - T_1\right)}{2*1000}\left[1.9464*10^{-6}\left(T_3^2 + T_1^2\right) + 4.4086*10^{-3}\left(T_3 + T_1\right) + 27.041\right]\frac{kJ}{rxn} \tag{16}$$

Total Required Heat Energy Input for Reaction III is:

$$Q = \left(-5.0807*10^{-6}T_3^2 + 1.2042*10^{-2}T_3 + 6.4257\right) + \left(\frac{\left(T_3 - T_1\right)}{1000}\left[1.9464*10^{-6}\left(T_3^2 + T_1^2\right) + 4.4086*10^{-3}\left(T_3 + T_1\right) + 27.041\right]\right)\frac{kJ}{rxn} \tag{17}$$

The required energy input of process I was calculated in the same manner. As discussed later, this energy is a negative value, signifying that heat must be removed from this exothermic reaction and from the reactants as they are cooled to the appropriate temperature. Figs. 7-9 show the required energy inputs of the three processes at various temperatures. The model additionally analyzes each energy demand by linearizing the temperature dependencies of the energy inputs and determining the derivative of the linear fit. Although, in actuality, the

derivative of the required energy input has the form of a first order polynomial and is dependent on temperature, the temperature-independent approximation used in the model provides a comparison between the three reactions of the effects on required energy inputs that changing the temperatures have. The temperatures for the processes were considered at 120°C, 850°C, and 400°C for processes I, II, and III, respectively.

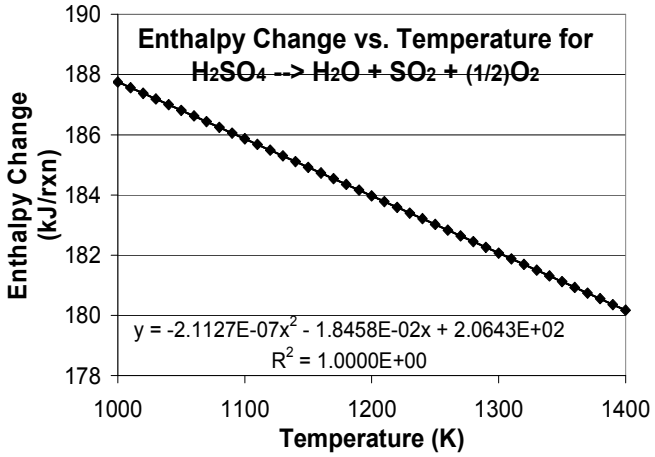

Fig. 5. Enthalpy change of reaction for Process II as a function of temperature.

The next portion of the model involved the heat transfer and heat exchanger design for the endothermic processes. The high temperature nature of the reactions, along with the corrosive natures of the reactants called for high temperature material. Hastelloy X was considered as the heat exchanger material, because of its ability to withstand corrosion of reactants such as sulfuric acid and high temperatures (> 1000°C). Additionally, Hastelloy X has very favorable heat transfer properties such as the thermal conductivity at high temperatures. The working fluid on the secondary loop in the plant is also helium gas. Helium does not compromise the integrity of the Hastelloy X pipes as it is a nobel gas and chemically inert at very high temperatures.

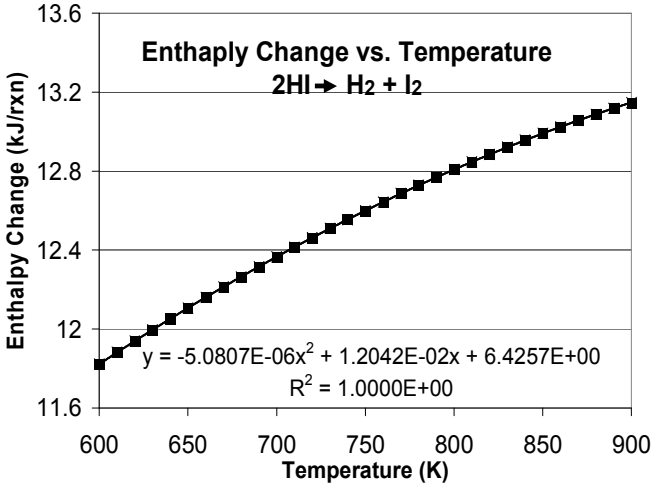

Fig. 6. Enthalpy change of reaction for Process III as a function of temperature.

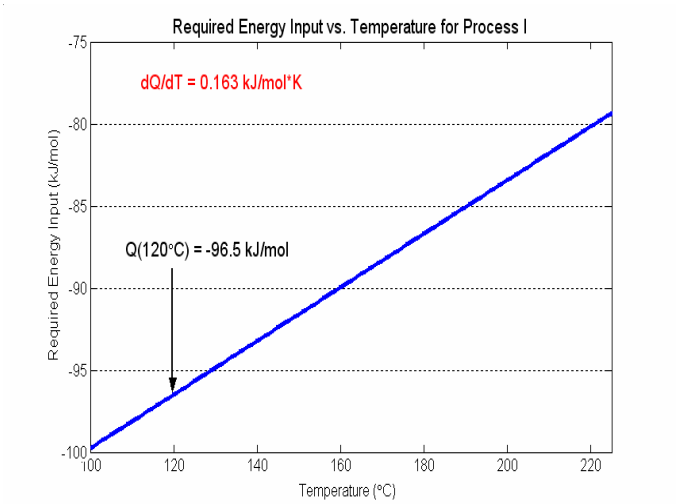

Fig. 7. Energy input of process I (negative because cooling is required) as a function of temperature as determined by the computational model. The derivative of a linearized data fit is shown.

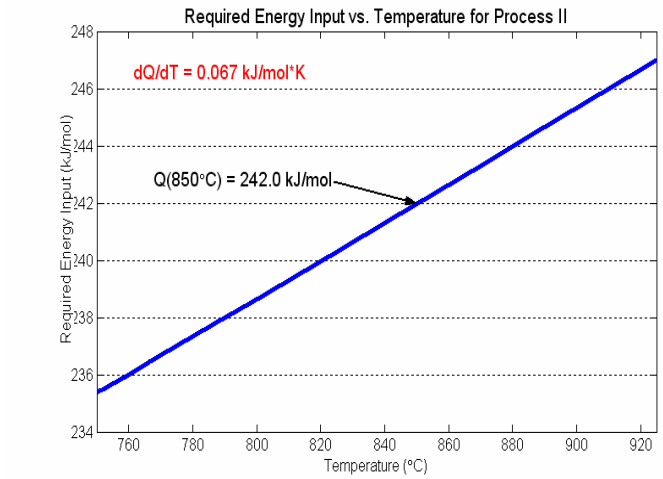

Fig. 8. Energy input of process II as a function of temperature as determined by the computational model. The derivative of a linearized data fit is shown.

Several different heat exchanger designs were considered, and a banked tube heat exchanger design was used [32]. As shown in Fig. 10, this design has favorable heat transfer characteristics and is economically feasible, industrially common, and versatile (variable number of pipes and surface area).

The flow properties of the gases were determined to apply appropriate heat transfer correlations. The computational model analyzed range of mass flow rates for both the helium and the reactant gas. Combination of various pipe sizes and number of pipes were used to compare heat transfer performance of the heat exchanger. In the final heat exchanger design, a nominal pipe size of 3/8" was used. The 1/8 and 1/4" pipes produced high flow velocities demanding prohibitively expensive pumping systems to generate the required head. The flow profile for a variable number of pipes in the heat exchanger and a variety of mass flow rates is shown in Fig. 11. As expected, as mass flow rate increases or the number of pipes decreases, the

flow velocity increases in each pipe [33]. The heat exchanger design was then analyzed in order to derive equations governing heat transfer in the heat exchanger. The macroscopic model shown in Fig. 12 was used for the tube of heat exchanger.

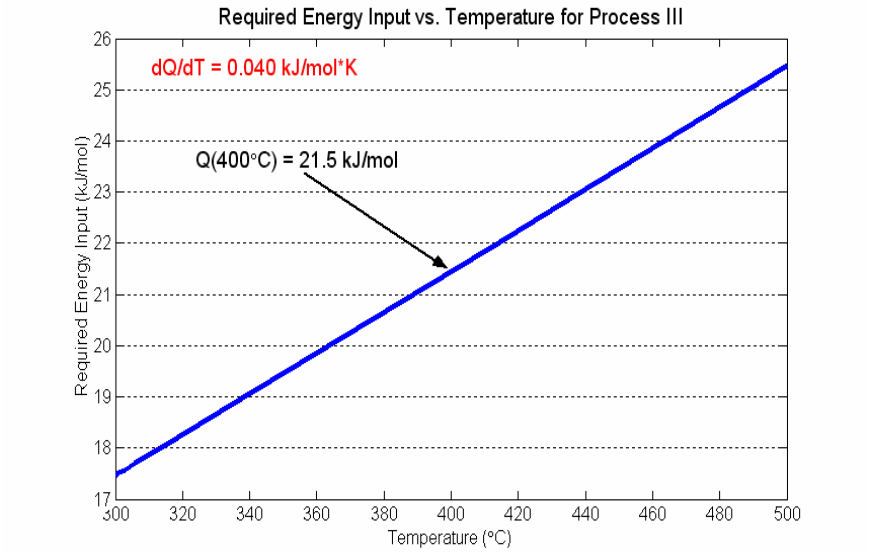

Fig. 9. Energy input of process III as a function of temperature as determined by the computational model. The derivative of a linearized data fit is shown.

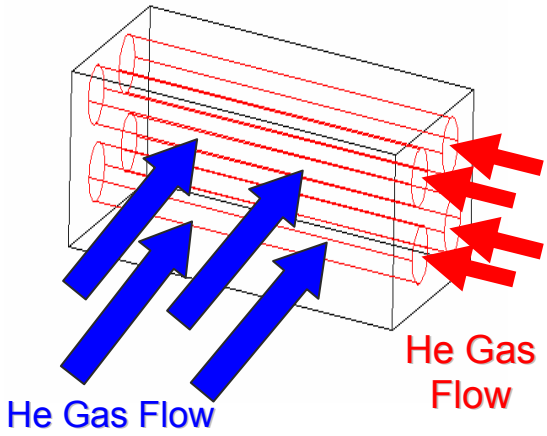

Fig. 10. Heat exchanger with flow across tube bed.

Three resistances to heat transfer from the helium gas to the gas reactants were considered: inner wall convection , conduction through the Hastelloy X , and outer wall convection. The equation governing heat transfer and the overall heat transfer coefficient were derived as follows:

$$q = U\left(2\pi r_o L\right)\left(T_{\infty,i} - T_{\infty,o}\right) \tag{18}$$

$$U^{-1} = \left(\frac{r_o}{r_i}\frac{1}{h_i}\right) + \left(r_o \frac{\ln\left(\frac{r_o}{r_i}\right)}{k_x}\right) + \left(\frac{1}{h_o}\right) \tag{19}$$

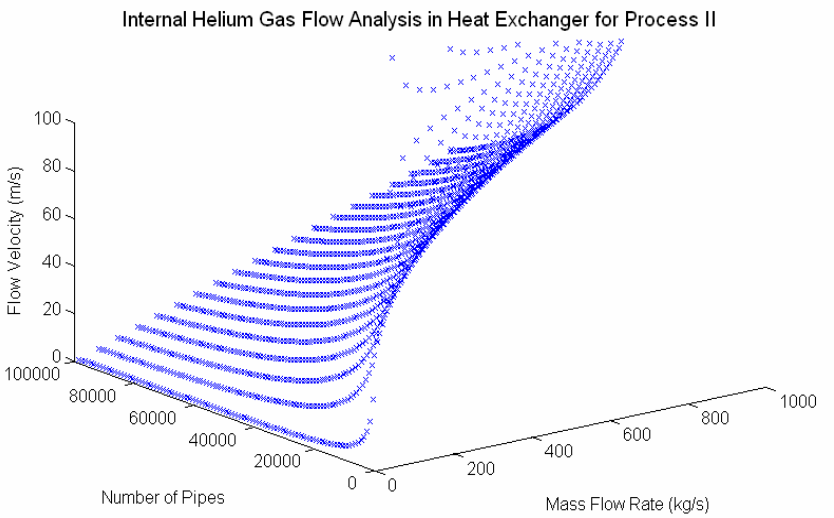

Fig. 11. Flow rate analysis for variable number of pipes in the heat exchanger and mass flow rate for Process II.

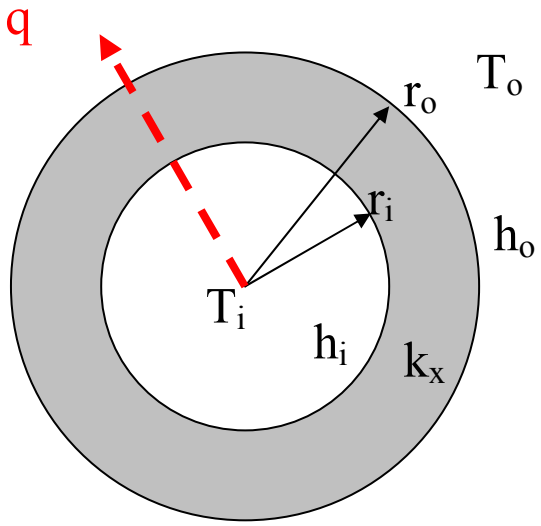

Fig. 12. Macroscopic heat exchanger schematic for tube of heat exchanger.

The Dittus-Boelter heat transfer correlation was used to determine the Nusselt number of the helium gas [34]. The comprehensive equation given by Churchill and Bernstein was then used to determine the Nusselt Number of the reactant gas on the outer surface of the pipes [34]. The constants in the above equations such as density, absolute viscosity, and specific heat were taken from Component Plus [35]. Fig. 13 compares the inner and outer wall heat transfer coefficients to the overall heat transfer coefficient. The heat transfer coefficient on the helium side of the heat exchanger is fairly high, while that of the side with the reactant gases is approximately an order of magnitude lower. The relatively high value of the helium heat transfer coefficient can be attributed to its high thermal conductivity, which is roughly five times higher than that of air and other common gases [35].

The overall heat transfer coefficients allow for one to analyze each particular flow regime combination and determine the amount of heat transferred from the helium to the reactant gas.

This amount of heat is of course dependent on the mass flow rate of helium, which is specified by the reactor size. For the PBMR reactor with 265 kW thermal power the mass flow rate, as discussed earlier, was 127.33 kg/s. This flow rate resulted in a heat transfer rate from the helium gas in Process II to the reactant gas of 66.12 MW. This amount of power corresponded to 24.95% of the total reactor power. As the helium gas passes to the heat exchanger for Process III, more energy is lost to the reactant gas in order to drive the decomposition of hydrogen iodine. The helium mass flow rate of 127.33 kg/s resulted in a heat transfer rate of 5.86 MW to the reactant gas in Process III. This corresponded to 2.21% of the total reactor power.

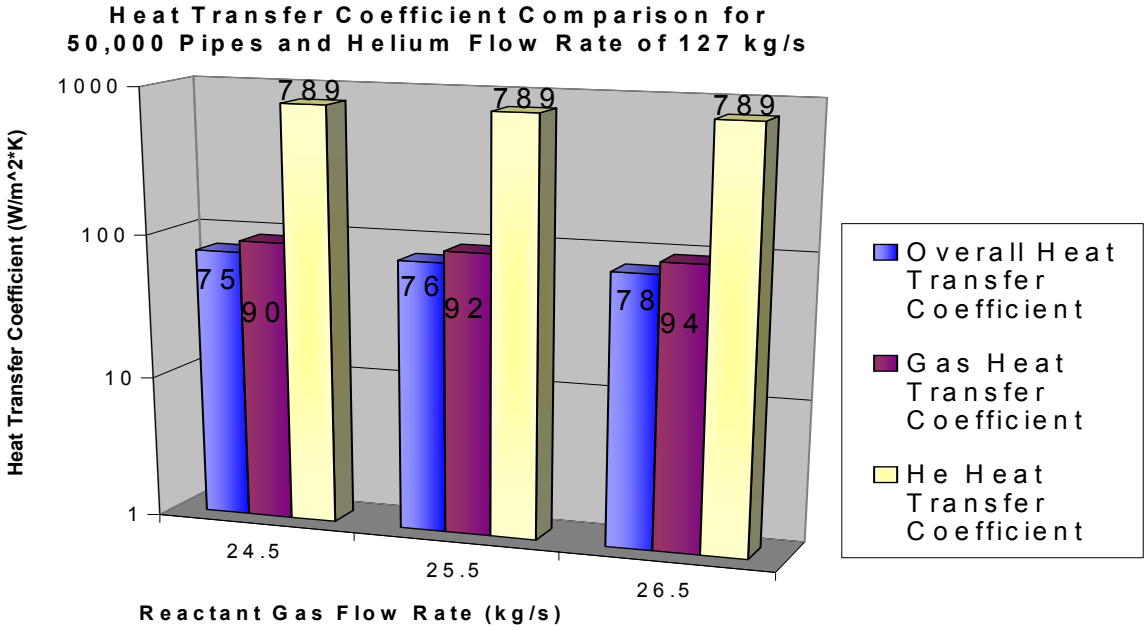

Fig. 13. Comparison of heat transfer coefficients for the outer wall, inner wall, and the overall system.

The computational model used the heat transfer rate to the reactant gas to determine the net amount of hydrogen produced. In this case, the plant was capable of producing 17.38 million kg of hydrogen gas per year (STP conditions assumed for mass calculation from the initial molar flow rate determination). This amount of hydrogen corresponded to 5.79×10^8 kWh of energy per year. Because the reactor produced 2.323×10^9 kWh of energy each year, the actually efficiency of the potential energy of the hydrogen gas in relation the energy produced by the reactor was 24.92%. This indicates that the majority of the energy put into producing hydrogen is indeed recovered, as only 2.24% if the reactor power that is put into producing hydrogen would be lost in this process.

Although this reactor was capable of generating a fairly significant amount of hydrogen each year, much of the reactor power would have been unrecoverable if the coolant was simply cooled to meet the reactor inlet temperature specification upon exiting the heat exchanger of Process III. To eliminate this excessive waste, cogeneration methods of producing both hydrogen and electricity were considered.

After exiting the second heat exchanger (i.e. that of Process III), the temperature of the coolant was 791.14°C. The reactor thermalhydraulic analysis required that the secondary loop inlet the primary-secondary heat exchanger at 500°C. Therefore, further cooling of the helium was necessary, and the Brayton cycle was studied to see if this cooling could result in net work output in the form of electricity. The proposed Brayton cycle is shown in Fig. 14. The isentropic efficiencies of both the turbine and compressor were assumed to be 85%.
The known state points in the Brayton cycle were points 3 and 2, which had temperatures of 791.14°C and 500°C, respectively. In addition, because of the constant pressure lines, points 2s, 2, and 3 had a pressure of 4.6 MPa, while points 1, 4, and 4s had pressures of 1.53 MPa. The pressure of 1.53 MPa was chosen because it is roughly 1/3 of the higher pressure at points 2s, 2, and 3, and this pressure ratio is realistically achievable for Brayton cycles operating between the proposed temperature ranges. Table 1, details the analysis of the Brayton cycle. All enthalpy and entropy values for helium were taken from Tsederberg et. al [36].

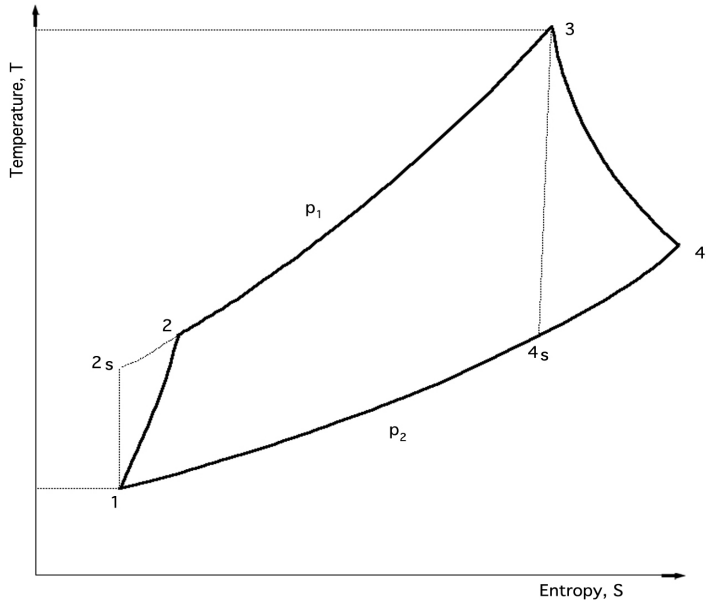

Fig. 14– Brayton cycle used to analyze cogeneration of electricity with the hydrogen production process. The isentropic efficiencies of the turbine and compressor were both assumed 85% to account for irreversibility in the system.

Table 1 – Brayton cycle analysis for cogeneration of electricity

Point	P (MPa)	T (°C)	S (kJ/kg·K)	h (kJ/kg)
1	1.53	183.10	-2.881	955.7
2s	4.6	450.00	-2.881	2351.1
2	4.6	500.00	-2.5076	2610.7
3	4.6	791.14	-0.8753	4121.9
4s	1.53	398.17	-0.8753	2072.5
4	1.53	437.67	-0.5787	2277.4

The ideal efficiency of the proposed cycle is 43.3%, and the actual efficiency is 12.5% after inefficiencies were considered. The non-ideal case resulted in a net power generation of 24.1 MW electrical from the cycle with the hydrogen mass flow rate of 127.33 kg/s. This net

rate of electricity generation is equivalent to placing 2.11×10^8 kWh of electricity on the grid each year. This power output represented 9.09% of the total reactor power. The resulting overall efficiency of the hydrogen and electricity production is 36.26%, when the Brayton cycle was considered.

Although the efficiency was not as high as initially expected for the given reactor specifications dictated by the thermalhydraulics analysis, the model predicted that the overall efficiency would increase to slightly over 45% by raising the maximum temperature of the helium on the secondary loop by 50°C. This raise in temperature, and therefore enthalpy, of the secondary fluid allowed more heat to be extracted in the hydrogen production process. The high temperature demands of the process limited the amount of heat that can be extracted from the helium, because excessive heat transfer would have causes the helium to begin to cool the reactant gas to below the required reaction temperature. However, by raising the helium temperature, more heat can be removed from the fluid, and the overall efficiency increased.

5. Conclusions

Through the neutronics and thermalhydraulic analysis of the reactor and development of the SI Process computational model, it was determined that the 265 MW thermal Pebble Bed Reactor could supply enough energy to produce 17.38 million kg of hydrogen per year. This amount of hydrogen corresponded to 5.79×10^8 kWh of energy per year. Through analyzing the SI Process with the computational model, it was determined that the helium transferred 66.12 MW to the reactant of Process II and 5.86 MW to the reactant gas in Process III. After the gas exited the second endothermic process, it was passed through a Brayton cycle with assumed turbine and compressor isentropic efficiencies of 85%. The Brayton cycle resulted in net power production rate of 24.1 MW electrical and an actual efficiency of 12.5%. This net power output corresponded to placing 2.11×10^8 kWh of electricity on the grid each year. The overall plant efficacy was determined to be 36.3%, and by increasing the maximum temperature on the secondary helium loop, it is anticipated that the overall efficiency would increase to over 45%.

6. Bibliography

1. Iwasaki W. A consideration of power density and hydrogen production and utilization technologies. Int J Hydrogen Energy 2003;28(12):1325-1332.
2. Energy Efficiency and Renewable Energy (EERE), US Department of Energy. http://www.eere.energy.gov 2003.
3. Lipovetsky V. Gaseous production by water dissociation method. Int J Hydrogen Energy 2003;28(4):377-379.
4. Stojic DL. Hydrogen generation from water electrolysis-possibilities of energy saving. J Power Sources 2003;88:1-5.
5. Levent M, Gunn DJ. El-Bousiffi MA. Production of hydrogen-rich gases from steam reforming of methane in an automatic catalytic microreactor. Int J Hydrogen Energy 2003;28(9):945-959.
6. Otsuka K, Yamada C, Kaburagi T, Takenaka S. Hydrogen storage and production by redox of iron oxide for polymer electrolyte fuel cell vehicles. Int J Hydrogen Energy 2003;28(4):335-342.
7. Kojima Y, Suzuki K, Fukumoto K, Sasaki M, Yamamoto T, Kawai Y, Hayashi H. Hydrogen generation using sodium borohydride solution and metal catalyst coated on metal oxide. Int J Hydrogen Energy 2002;27(10):1029-1034.

8. Amendola SC, Sharp-Goldman SL, Janjua MS, Spencer NC, Kelly MT, Petillo PJ, Binder M. An ultrasafe hydrogen generator: aqueous, alkaline borohydride solutions and Ru catalyst. J Power Sources, 2000;85:186-189.
9. Besenbruch GE. General Atomic sulfur-iodine thermochemical water-splitting process. Am. Chem. Soc., Div. Pet. Chem., Prepr. 1982;271:48–53.
10. Hwang G, Onuki K. Simulation Study on the Catalytic Decomposition of Hydrogen Iodide in a Membrane Reactor with a Silica Membrane for the Thermochemical Water-Splitting IS Process. J Membrane Science 2001;194:207-215.
11. Norman JH, Besenbruch GE, O'Keefe DR. Thermochemical water-splitting for hydrogen production. Gas Research Institute Report GRI-80/ 0105, 1981.
12. Norman JH, Besenbruch GE, Brown LC, O'Keefe DR, Allen CL. Thermochemical water-splitting cycle bench-scale investigations and process engineering. General Atomic Report GA-A 16713, 1982.
13. Forsberg C, Pickard PS, Peterson P. The advanced high temperature gas reactor for production of hydrogen or electricity. Nuclear News Feb. 2003. p. 30.
14. Engels H, Knoche KF, Roth M. Direct dissociation of hydrogen iodide—an alternative to the general atomic proposal. Proceedings of the 6th World Hydrogen Energy Conference. Vienna Austria. 2 July 1986. p. 657.
15. Nakajima H, Ikenoya K, Onuki K, Shimizu S. Closed cycle continuous hydrogen production test by thermochemical IS process. Kagaku Kougaku Ronbunshu 1998;24 (2):352-359.
16. Onuki K, Shimizu S, Nakajima H, Fujita S, Ikezoe Y, Sato S, Machi S. Studies on an iodine-sulfur process for thermochemical hydrogen production. Proceeding of the 8th World Hydrogen Energy Conference, Honolulu, 1990. p. 547-56.
17. Onuki K, Nakajima H, Shimizu S, Sato S, Tayama I. Materials of construction for the thermochemical IS process (I). J Hydrogen Energy System Society of Japan 1993;18(2):49-56.
18. Nakajima H, Sakurai M, Ikenoya K, Hwang GJ, Onuki K, Shimizu S. A study on a closed-cycle hydrogen production by thermochemical water-splitting IS process. in: Proceedings of the 7th International Conference on Nuclear Engineering,, ICONE-7104Tokyo, Japan, April 1999.
19. Sakurai M, Nakajima H, Onuki K, Shimizu S, Investigation of 2 liquid phase separation characteristics on the iodine-sulfur thermochemical hydrogen production process J. Membr. Sci. 1999;156:61-71.
20. Sakurai M, Bilgen E, Tsutsumi A, Yoshida K, Adiabatic, UT-3 thermochemical process for hydrogen production. Int J Hydrogen Energy 1996;21(10):865-870.
21. Tadokoro Y, Kajiyama T, Yamaguchi T, Sakai N, Kameyama H, Yoshida K. Technical evaluation of UT-3 thermochemical hydrogen production process for an industrial scale plant. Int J Hydrogen Energy, 1997;22(1):49-56.
22. Brown LC, Besenbruch GE, Schultz KR, Showalter SK, Marshall AC, Pickard PS, Funk JF. High Efficiency Generation Of Hydrogen Fuels Using Thermochemical Cycles And Nuclear Power. AIChE 2002 Spring National Meeting, Topical TH - Nuclear Engineering, Session THa01 139 New Orleans, LA, March 11-15, 2002.
23. Nifenecker H, David S, Loiseaux JM, Giorni A. Hybrid Nuclear Reactors. Progress in Particle and Nuclear Physics, 1999:43(1):683-827.
24. Southworth F. Very-High-Temperature Reactor. Idaho National Engineering and Environmental Laboratory. http://energy.inel.gov/gen-iv/vhtr.html 2003.
25. Nicholls D. Status of the pebble bed modular reactor. Nuclear Energy 2000; 39(4) Aug., 231-236
26. William KT, editor. Modular Pebble-Bed Reactor Project, FY 2001 Annual Report. INEEL/EXT-01-01623, Idaho Falls, Idaho. December 2001.
27. Croy C, Elkhiamy S, Kopenec R Revankar ST. Scaling Investiation of a Modualar Pebble Bed Optimization. School of Nuclear Engineering Purdue University, Senior Design Report 2001.
28. Joo H, Barber D, Jiang G, Downar T. PARCS: A Multi-Dimensional Two-Group Reactor Kinetics Code Based on the Nonlinear Analytic Nodal Method. Purdue University, School of Nuclear Engineering Report PU/NE-98-26, 1998.
29. Downar T, Lee DJ. Comparative Analysis of PBMR Core Physics Test Problems. ANS M&C Meeting, Gatlinburg, TN, April 6, 2003.
30. Fenech H. Heat Transfer and Fluid Flow in Nuclear Systems, Pergamon Press, 1980, pp. 382-401.
31. HSC Chemistry 5 v5.1 Outokumpu Research Oy 2002.
32. Gupta, JP. Working with Heat Exchangers: Questions and Answers. Hemisphere Publishing Co. 1990, pp. 257-288.
33. Mcdonald AT, Fox RW. Introduction to Fluid Mechanics 5th Ed. John Wiley and Sons Inc. 1998.

34. Incorpera FP, Dewitt DP. Fundamentals of Heat and Mass Transfer 5th Ed. John Wiley and Sons. 2002.
35. Component Plus v 3.4.0.1 Prosim SA, 2001.
36. Tsederberg NV, Popov VN, Morozova, NA. Thermodynamic and Thermophysical Properties of Helium. Translated from Russian. U.S. Department of Commerce, National Bureau of Standards. 1971.